Journal of Magnetism and Magnetic Materials 511 (2020) 166963

Contents lists available at ScienceDirect

Journal of Magnetism and Magnetic Materials

journal homepage: www.elsevier.com/locate/jmmm

Research articles

Negative capacitance of nanocomposites with CoFeZr nanoparticles embedded into silica matrix

J.A. Fedotova[a], A.V. Pashkevich[a,b], Ali Arash Ronassi[c], T.N. Kołtunowicz[d,*], A.K. Fedotov[a], P. Zukowski[d], A.S. Fedotov[b], J.V. Kasiuk[a], Yu.E. Kalinin[e], A.V. Sitnikov[e], V.V. Fedotova[f], A. Evtuh[g]

[a] Institute for Nuclear Problems of Belarusian State University, Minsk, Belarus
[b] Belarusian State University, Minsk, Belarus
[c] Payame Noor University, Tehran, Iran
[d] Lublin University of Technology, Lublin, Poland
[e] Voronezh State Technical University, Voronezh, Russia
[f] Practical-Scientific Center of NASB on Material Science, Minsk, Belarus
[g] Institute of Semiconductor Physics, Kiev, Ukraine

ARTICLE INFO

Keywords:
Granular nanocomposites
Silica matrix
"Core-shell" structure of nanoparticles
Electrical properties
Magnetization
Negative capacitance

ABSTRACT

The study presents frequency dependences of real part of admittance $Z'(f)$ and phase shift angle $\theta(T, f)$ in nanogranular films containing CoFeZr nanoparticles with "core-shell" structure embedded into SiO_2 matrix. The 3 μm thicknesses $(Co_{41}Fe_{49}Zr_{10})_x(SiO_2)_{100-x}$ films with $20 \leq x \leq 80$ at.% were deposited in vacuum chamber evacuated either with pure Ar (Set 1 samples) or Ar + O_2 gas mixture (Set 2) using ion-beam sputtering technique. After characterization by X-Ray diffraction, Mössbauer spectroscopy, scanning electron microscopy and magnetization studies, the films both of Set 1 and Set 2 samples were subjected by admittance measurements at 300 K in the frequency range of 0.1–1000 kHz. Mössbauer spectroscopy have shown that oxidized CoFeZr nanoparticles in Set 2 samples contain semiconducting iron-based oxides with Fe^{3+} charge states of iron ions. The observed $Z'(f)$ and $\theta(f)$ dependencies for the Set 2 films below the x_c have shown dielectric regime of carrier transport. They also exhibited that at weak AC electric fields inductive-like contribution to reactive part of admittance (with positive θ values) prevails over the capacitive one $f > 10$ kHz. This effect of the so-called "negative capacitance" was explained by the delay of current, formed by electrons hopping between nanoparticles, relative to applied bias voltage. This delay is forced by formation of dipoles of charged FeCoZr nanoparticles with native Fe-based oxide "shells" around them that results in the increase of mean life time of hopping electrons on nanoparticles with "core-shell" structure.

1. Introduction

Nowadays the synthesis and investigation of the materials, usually called the granular nanocomposites, are of a great interest for the material engineering and also magnetoelectronic applications [1]. Particular attention is given to the nanocomposites in which nanosized particles of soft ferromagnetic alloys are randomly distributed in dielectric matrix. The interest to such systems is mainly due to wide possibilities of their application (e.g. for magnetic saving and recording of information, for engineering of protecting screens against the electromagnetic radiation, in highly-Ohmic resistors, and for other purposes) [2]. The fact that some of nanogranular composites possess the semiconducting properties but their manufacturing is frequently cheaper, determines the possibility to use them as active and reactive electrical circuit components and also in sensors and transducers. At the same time, some of such nanocomposites are characterized by unusual combination of magnetic and electric properties [3], such as giant magnetoresistance, high values of remanence, the change of resistivity in a wide range, inductive-like reactive impedance, etc [4–14].

Also it should be stressed that the metal-dielectric nanocomposites are the interesting model systems to study such important and fundamental effects as percolation and hopping conductance, weak localization at low temperatures, etc [14–17]. The particular contribution of each of these charge carriers transport mechanisms, that are realized in

* Corresponding author.
E-mail address: t.koltunowicz@pollub.pl (T.N. Kołtunowicz).

https://doi.org/10.1016/j.jmmm.2020.166963
Received 19 November 2019; Received in revised form 19 March 2020; Accepted 30 April 2020
Available online 04 May 2020

the binary metal-dielectric nanocomposites, is strongly dependent on the volume ratio of the metallic and dielectric phases, and also on phase and magnetic structure of nanoparticles embedded into dielectric matrix [1]. As a result, when the metallic fraction x increases, the binary metal-dielectric composite will pass from the weakly-conductive (dielectric) to the highly-conductive (metallic) state. In such composites this takes place when some critical concentration of metallic phase x_C is reached (when continuous conducting percolating cluster is formed from the contacting metallic particles). The mentioned critical concentration x_C is called the percolation threshold [1,4]. In this case, when $x < x_C$ (below the percolation threshold) the binary composite will be at the dielectric side of the metal-insulator transition (MIT) whereas at $x > x_C$ (beyond the percolation threshold) composite is at the metallic side of MIT.

But if phase structure of metallic nanoparticles is more complicated and includes not only metallic phase "core", but also semiconducting "shell", the description of temperature/frequency dependences of admittance becomes strongly different from percolation theory [1,4]. For non-binary nanocomposites with "core-shell" structure of highly-conductive nanoparticles, two critical values of x are observed. With the increase of x, the threshold of "touching" is attained firstly, when at $x \approx x_C$ (as for binary composites) the neighboring "shells" of nanoparticles begin to adjoin with each other (we call it the "touching threshold" x_t). And, in accordance with [14,17], real percolation threshold x_C in such non-binary nanocomposites is achieved only at much higher x values (about 60–70 at.%). As was observed earlier in our experiments, just such nanocomposites, where "shells" from native oxides of Fe around CoFeZr nanoparticles are semiconducting, possess by "negative capacitance" effect resulting in the delay of current relative to applied AC bias voltage [1,5,6,8–13].

Therefore, the main goal of this paper is to investigate the influence of atmosphere of deposition (pure Ar or gas mixture Ar + O_2) and relation of metallic and dielectric constituents on phase structure and frequency dependences of admittance in granular nanocomposites consisting of the nanoparticles of FeCoZr alloy embedded into amorphous dielectric silica matrix.

2. Experimental

Granular $(Co_{41}Fe_{49}Zr_{10})_x(SiO_2)_{100-x}$ nanocomposites were prepared using ion-beam sputtering of compound target (containing alloy CoFeZr plate covered with quartz stripes with changing distances between them, (see, [1,14] in details) in vacuum chamber filled with either pure Ar (Set 1 samples) under the pressure $p_{Ar} = 0.80$ mPa or Ar + O_2 gas mixture (Set 2 samples) under partial pressures $p_{Ar} = 0.82$ mPa and $p_O = 0.032$ mPa. The samples under consideration were the films of about 3 μm thicknesses deposited on glass ceramic substrates. The used method allowed to obtain the whole array of samples with different FeCoZr alloy concentrations in the range of 20 at.% $< x <$ 80 at.%.

Morphology and chemical composition of CoFeZr-SiO_2 films was carried out on a Scanning Electron Microscope (SEM) LEO 1455VP Oxford Instruments, equipped with a Rontec attachment for quantitative and qualitative energy dispersive X-ray (EDX) microanalysis. EDX measurements have shown that the content of the metallic phase x in $(Co_{41}Fe_{49}Zr_{10})_x(SiO_2)_{100-x}$ films varied in the range of 20–80 at.% from one to another ends of the substrate. The error in estimation the concentration of atoms in the metallic phase in nanocomposite films did not exceed 2 at.%.

Studies of local configurations of Fe ions, which provide information on the phase composition and magnetic state of iron-containing nanoparticles in composite films, were carried out using the Mössbauer spectroscopy on ^{57}Fe isotope. These measurements were carried out on an SEE CO Mossbauer spectrometer (USA) operating in the transmission mode. For Mössbauer measurements, the films were deposited on aluminum foil with the thickness 0.1 mm. ^{57}Co was used as a source of γ-radiation in the Rh matrix with an activity of 25 mCi. The obtained spectra were fitted using the MOSMOD code, which assumes an approximation of the subspectra corresponding to individual local configurations of Fe by Voigt functions (convolution of Lorentz and Gauss functions). The code allows to take into account the distribution of the values of the isomeric shift δ and quadrupole splitting Δ. The δ values are given relative to pure α-Fe. The half-width of the Lorentz line, which were used to interpret the spectra, was fixed and equal to 0.15 mm/s.

X-ray diffraction (XRD) analysis of $(Co_{41}Fe_{49}Zr_{10})_x(SiO_2)_{100-x}$ films was performed on an Empyrean PANalytical diffractometer using characteristic Cu-K_α X-ray radiation ($\lambda = 0.154056$ nm), a graphite as monochromator and X'Celerator detector. Diffraction patterns were recorded at a constant angle of incidence of 5° relative to the film surface and scanning in the range of reflection angles $2\Theta = 10°–120°$. The instrumental widening of the lines was estimated using diffraction patterns of the reference sample LaB_6. The lattice parameters a were determined on the basis of the angular positions 2Θ of maxima of the diffraction pattern using the FullProf code based on the Ritveld method [18]. Sizes of coherent scattering regions D_K were estimated using the Scherer formula [19].

The dependences of the magnetic moments μ on magnetic fields with induction B of composite films were obtained on VSM-PPMS (Quantum Design) vibration magnetometer in the temperature range $T = 2–350$ K and magnetic fields $B = 0–8$ T with instrumental error not higher than 0.02%. The temperature in the vicinity of the sample to be measured in the close-cycled cryostat was determined with an accuracy of 0.001 K.

The admittance at 300 K was measured on rectangular 2×10 mm^2 samples provided with ultrasonically soldered indium contacts. Admittance of the samples was measured by a 4-probe method using precise RLC-meters Agilent E4980A and Agilent E4285A (with probe voltage magnitude of 40 mV and standard correction procedure). This allowed to conduct measurements of current amplitude and phase in the frequency range 100 Hz $< f <$ 30 MHz with the following calculating of real/imaginary parts of admittance and phase shift angles [6–9]. Correction of the open circuit voltage mode was done with a pure glass ceramic substrate provided by contacts placed in the same geometry as for the nanocomposite films deposited on similar substrate. The relative error of admittance measurements was not more than 5%.

3. Chemical composition, phase structure, local atomic order and magnetometry of nanocomposite films

EDX measurements have shown that the chemical composition of metallic alloy in the composite films was $Co_{41}Fe_{49}Zr_{10}$ in at.%.

SEM studies of the films confirmed the presence of a nanogranular structure. In particular, Fig. 1 shows examples of SEM images for 3 samples of $(Co_{41}Fe_{49}Zr_{10})_x(SiO_2)_{100-x}$ films with different ratio of metallic (x) and dielectric (100-x) phases. The dark areas on these images, recorded in the secondary electrons mode, correspond to the metallic phase of $Co_{41}Fe_{39}Zr_{20}$, while the light areas are associated with SiO_2 matrix. Estimation of the average size of granules indicates that the growth of x in the composite films leads to the change in the granules diameter. In particular, the increase of x from 30 to 59 at.%, the granules diameter increases on average from 2 to 7 nm. Authors of papers [17,20] noted that for the most metal-dielectric nanocomposites this dispersion could reach 25–30%.

The presented in Fig. 1a electron diffraction patterns display that for nanocomposite films with small x values we can see two halos that differ significantly in diameter. The halo of a smaller diameter corresponds to the dielectric phase. This follows from an estimation of the average interatomic distance, which we can determine from the "dielectric" halo diameter using the method proposed in [18]. The halo of a larger diameter is formed due to electron beam diffraction on metallic particles. This follows from the fact that the average interatomic

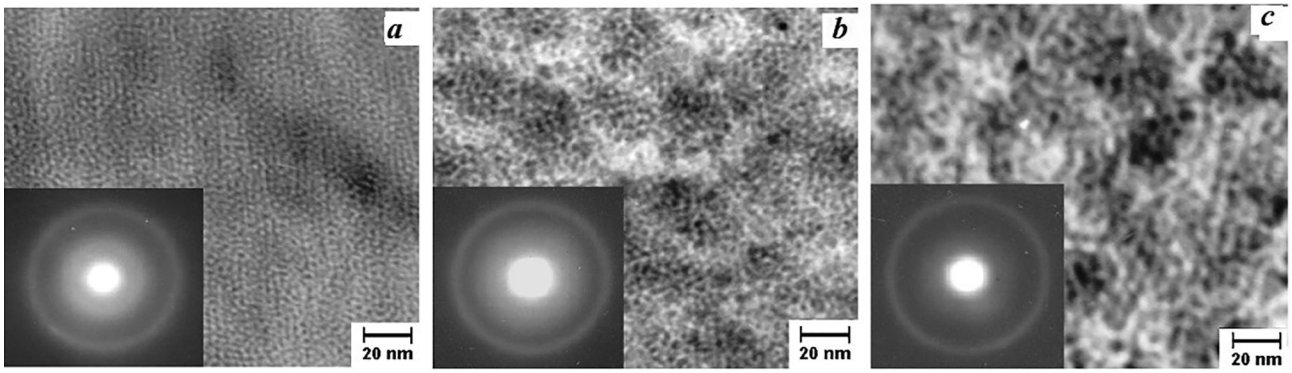

Fig. 1. SEM images and electron diffraction patterns for granular nanocomposites $(Co_{41}Fe_{49}Zr_{10})_x(SiO_2)_{100-x}$ films with x = 30 at.% (a), 44 at.% (b) and 52 at.% (c).

distances calculated from the diameter of this "metallic" halo have intermediate values of the interatomic distances for the *bcc* lattice of Co and Fe. The intensity of the "dielectric" halo rapidly decreases with the increase of the metallic phase concentration x, so that for the samples with $x \approx 50$ at.%, on the diffraction patterns only the halo with larger diameter is identified (Fig. 1c).

These arguments are confirmed also by XRD patterns. As is seen from Fig. 2, in the composite films with x = 35 at.% (a) and 67 at.% (b) we observe a broad peak at $2\Theta = 44.7^{\circ}$, belonging to CoFeZr nanoparticles, that corresponds to the presence electron diffraction "metallic" halo shown in previous Fig. 1. A strong broadening of this diffraction line may indicate either small nanoparticle sizes or strong structural disordering. A significantly greater broadening is characteristic for this peak on the XRD pattern for x = 35 at.%, since, in accordance with the electron diffraction patterns, it contains nanoparticles of minimal size (Fig. 1a). In addition to this peak, the XRD pattern of the film with x = 35 at.% detects a broadened line of greater intensity at $2\Theta \sim 23^{\circ}$, which probably refers to the SiO_2 matrix, which is dominant in the film of this composition. In addition to the described diffraction lines, there is also a series of narrow lines from the glass ceramic substrate (including also SiO_2), denoted by asterisks (*) in Fig. 2a. The intensity of lines formed by the SiO_2 matrix and substrate is significantly reduced in the film with the composition x = 67 at.%. Instead, an additional line appears from the structure of CoFeZr nanoparticles ($2\Theta = 82.4^{\circ}$) on the corresponding XRD pattern. The approximation of XRD pattern for the film with x = 67 at.% is shown in Fig. 3. This approximation allowed to determine the following structural parameters, which characterize CoFeZr nanoparticles: the *bcc* lattice parameter $\alpha = 0.2865$ nm, which is close to the corresponding parameter for α-Fe ($\alpha_{Fe} = 0.28664$ nm [21]) and the alloy α-$Fe_{50}Co_{50}$ ($\alpha_{FeCo} = 0.28550$ nm [22]), as well as the size of coherent scattering

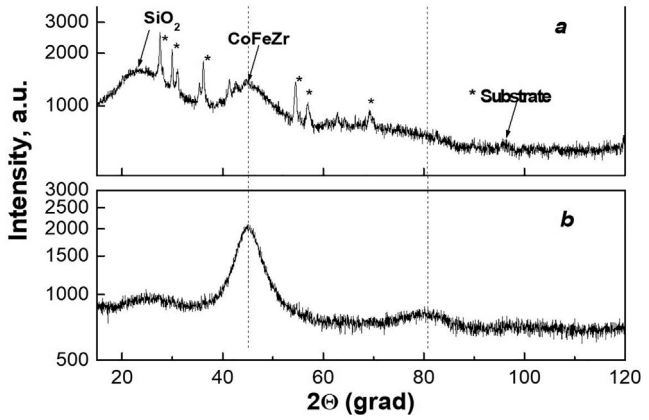

Fig. 2. XRD patterns for granular nanocomposites $(Co_{41}Fe_{49}Zr_{10})_x(SiO_2)_{100-x}$ with x = 35 at.% (a) and x = 67 at.% (b).

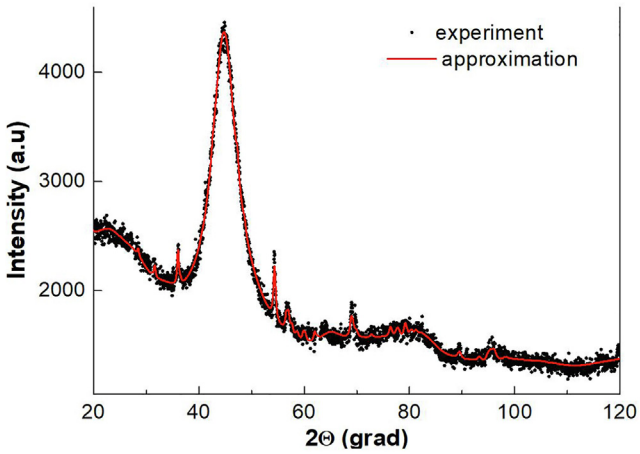

Fig. 3. Experimental (points) and approximated (red line) XRD patterns for the composite film $(Co_{41}Fe_{49}Zr_{10})_{67}(SiO_2)_{33}$. (For interpretation of the references to colour in this figure legend, the reader is referred to the web version of this article.)

regions (i.e., dimensions of crystallites or nanoparticles) $D_{coh} \sim 1.1$ nm.

Since, as shown by SEM (Fig. 1c), the size of nanoparticles in the film of similar composition is about 5 nm (i.e. much higher), we can attribute the detected broadening of diffraction lines by structural disorder in nanoparticles. The separation in the broadening of diffraction lines of the contributions from the dimensional component and from the stress component is not possible using this approximation due to small number of peaks from CoFeZr nanoparticles.

To study the local structural order of conducting nanoparticles and their possible phase composition, we used method of Mossbauer spectroscopy, which allows one to study materials that possess only short-range order. Fig. 4 shows the Mossbauer spectra of $(Co_{41}Fe_{49}Zr_{10})_x(SiO_2)_{100-x}$ films with different x values. Table 1 presents hyperfine parameters characterizing the phases found in the films by approximating the corresponding spectra.

As is seen in Fig. 4, Mossbauer spectra of all three films studied display three subspectra. The D1 doublet relates to the non-oxidized "core" of iron-based phase and the D2 doublet characterizes iron oxide with Fe^{3+} charge state of iron ions. The wider doublet D3 (or its singlet S), belonging to the oxide phase with variable oxidation state, characterizes variable-valence iron state. The relative contribution of mentioned subspectra varies with the changing of metallic nanoparticles concentrations x.

The spectrum for the sample with the x = 20 at.% in Fig. 4a contains the minimal portion of the D1 doublet (~24%), i.e. this sample has the minimal amount of non-oxidized iron phase. With the increase of the metallic fraction x, the content of the non-oxidized phase increases to 30% for x = 48 at.% and to 42% for x = 67 at.% (Table 1).

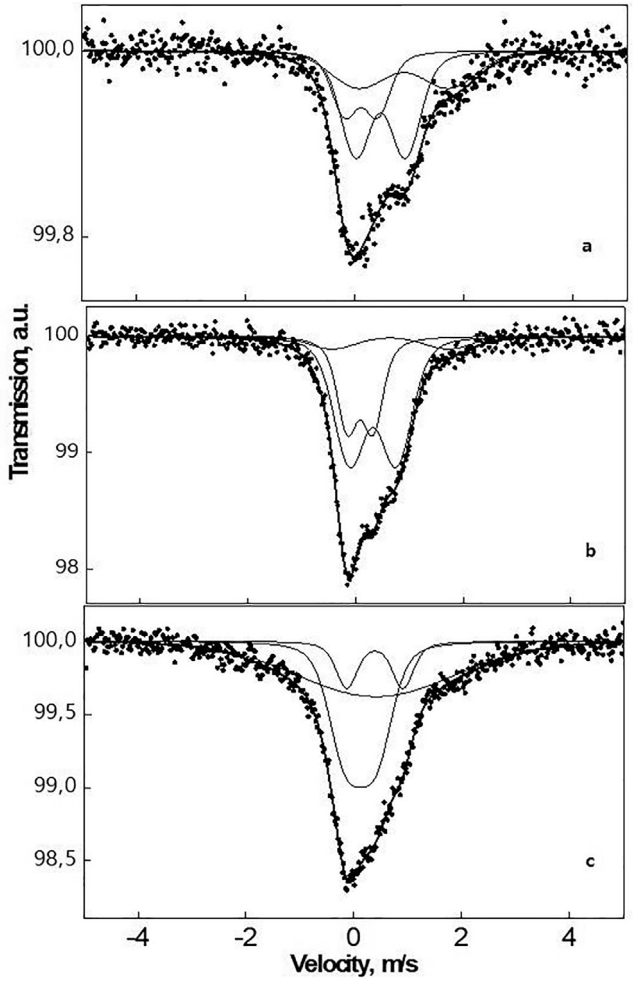

Fig. 4. Mossbauer spectra of nanocomposite films $(Co_{41}Fe_{49}Zr_{10})_x(SiO_2)_{100-x}$ with $x = 20$ at.% (a), 48 at.% (b) and 67 at.% (c), measured at 300 K, after annealing on air.

Table 1
Ultrafine parameters of the Mossbauer spectra of films $(CoFeZr)_x(SiO_2)_{100-x}$ at 300 K: δ – the isomeric shift, Δ – quadrupole splitting, σ – the line width, A – the contribution of the sub-spectrum.

x, at.%	Sub-spectrum	δ, mm/s	σ, mm/s	Δ, mm/s	*A*, %	Valence state of Fe (phase)
20	doublet D_1	0.12	0.61	0.35	24	Fe^0
	doublet D_2	0.48	0.44	0.91	47	$Fe^{3+}O$
	doublet D_3	0.90	1.65	0.93	29	$Fe^{2+}O$
48	doublet D_1	0.09	0.48	0.25	30	Fe^0
	doublet D_2	0.33	0.87	0.48	61	$Fe^{3+}O$
	doublet D_3	0.64	2.16	0.77	9	$Fe^{2.5+}O$
67	doublet D_1	0.12	0.49	0.56	42	Fe^0
	doublet D_2	0.39	0.27	1.05	12	$Fe^{3+}O$
	singlet *S*	0.41	2.85	0	46	$Fe^{3+}O$

Simultaneously with the increase of the amount of the non-oxidized CoFeZr phase when increasing *x*, there is a gradual decrease in the contribution of the doublet D2 (Fe^{3+}) from 47% at $x = 20$ at.% to 12% at $x = 67$ at.%. It should be noted also that the charge state of iron in the phase, described by the broadened doublet D3 (singlet S), changes from Fe^{2+} for the film with $x = 20$ at.% to Fe^{3+} in the spectrum of the sample with $x = 67$ at.%. Therefore, in the sample with $x = 67$ at.%, this sub-spectrum with the high width of the spectral line is a magnetically-collapsed sextet, i.e. oxide phase contains Fe^{3+}, in which magnetic interactions begin to appear (magnetic ordering due to the increasing sizes of the regions occupied by this phase). In other words, the total contribution of sub-spectra describing the phase with Fe^{3+} in the superparamagnetic (doublet D1) and partially magnetically ordered (singlet S) states equals 58%. This means that we can not speak about the decrease of the contribution of Fe^{3+} (semiconducting) oxides with *x* increasing from 48 at.% to 67 at.%, but only about its partial magnetic ordering. Attention should be paid also to the gradual shift of the D3 doublet (singlet S) to a lower velocity region when increasing *x*. In other words, according to the value of its isomeric shift, this sub-spectrum characterizes iron oxide with the valence of 2+ in films with small *x*, oxide with the valence of 2.5+ in the film with intermediate $x = 48$ at.%, and finally iron oxide with the valence 3+ in the film with maximal $x = 67$ at.%.

Therefore, in the studied nanocomposites, "additional oxidation" of the FeO type oxide to the α-Fe_2O_3 oxide, which is stable and maximally saturated with oxygen, occurs with the increasing of *x*, through the intermediate stage, i.e. Fe_3O_4 oxide. Thus, the film with $x = 20$ at.% contains iron in three different modifications – non-oxidized iron (in the metallic "core" of nanoparticles), dielectric iron oxide α-Fe_2O_3 (with the charge state of iron Fe^{3+}) and semiconducting iron oxide FeO (with the charge state of iron Fe^{2+}). The film with $x = 67$ at.% contains iron only in two phase states – non-oxidized iron and dielectric iron oxide α-Fe_2O_3 with Fe^{3+} charge state. Partial oxidation of nanoparticles indicates on correctness of the model "non-oxidized core-oxide shell" for their structure. In the case of the film with $x = 20$ at.%, we observe additional layer-by-layer oxidation of the nanoparticles when an intermediate layer of FeO oxide between the "non-oxidized core" and the outer "oxide shell α-Fe_2O_3" is formed. This sequence of nanoparticles oxidation when *x* changing is fully consistent with the model described earlier for FeCoZr nanoparticles embedded in the Al_2O_3 [10] or CaF_2 [23] matrixes. Thus, as follows from Table 1, over the entire *x* range of 20–67 at.%, the degree of oxidation of the alloy nanoparticles decreases with *x* increasing. The latter is logical to associate with the fact that smaller particles are oxidized to a greater degree (due to the greater specific surface).

The magnetization curves μ(*B*) of $(Co_{41}Fe_{49}Zr_{10})_x(SiO_2)_{100-x}$ composite films with varying content of metal nanoparticles $x = 23$ at.%, 49 at.% and 67 at.%, measured at different temperatures in the range $T = 5$–300 K, are presented in the Fig. 5. It should be noted that the film samples of different compositions are characterized by substantially different shape of μ(*B*) curves. For example, the μ(*B*) curves for the film with minimal content of metal fraction $x = 23$ at.% demonstrates practically linear shape (i.e. paramagnetic state) in almost the entire range of measured temperatures with a predominance of the ferromagnetic (blocked superparamagnetic) contribution at low $T = 6$ K. Such behavior of the magnetization curves indicates the small size of nanoparticles, and also, perhaps, their weak ferromagnetic properties, which are possible in the case of strong oxidation FeCoZr nanoparticles and the formation of weakly magnetic oxides of Fe and Co.

The increase of *x* values in the films leads to the increase of ferromagnetic contribution to magnetization curves, which is reflected in the increase in their magnetic moment, the coercivity H_C at low temperature, as well as the change in the shape of the μ(*B*) curves, that were close to saturation in high magnetic fields over the wide range of temperatures.

These changes are consistent with the results of data of XRD, electron beam diffraction and Mossbauer spectroscopy, which revealed the growth of the non-oxidized (ferromagnetic) nanoparticle "core" with increasing *x*. At the same time, like the Mossbauer spectroscopy, magnetometric studies indicate predominantly superparamagnetic state of non-oxidized nanoparticles even in the film with maximal $x = 67$ at.% in Fig. 4c, as indicated by a significant increase in H_C at low *T*, as well as the *S*-shaped form of μ(*B*) dependences at temperatures close to 300 K.

The frequency dependences of the active admittance *Z′* and phase

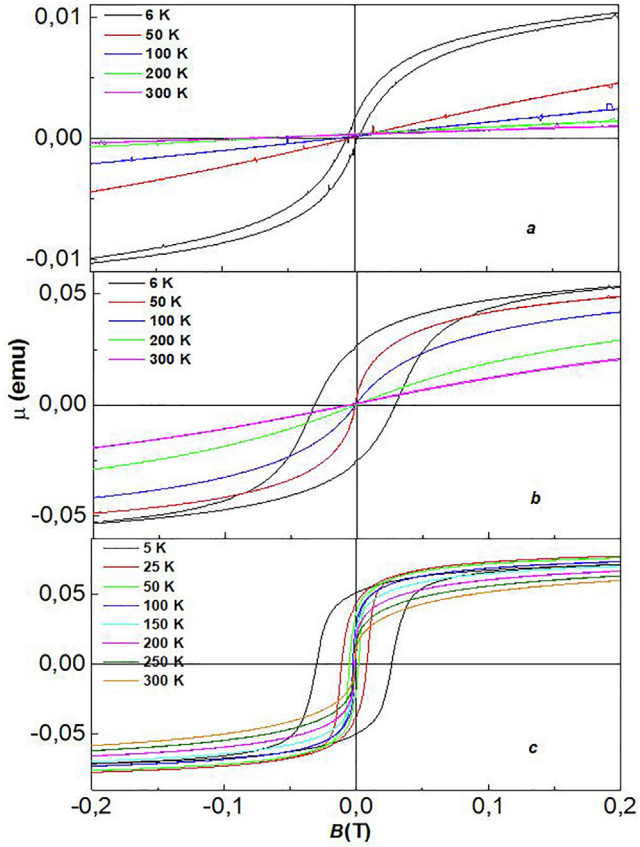

Fig. 5. Magnetization curves μ(B) of the $(Co_{41}Fe_{49}Zr_{10})_x(SiO_2)_{100-x}$ films with varying content of metal nanoparticles x = 23 at.% (a), 49 at.% (b) and 67 at.% (c), measured at different temperatures.

shift angle θ at 300 K for the film samples deposited in an atmosphere of pure argon are presented in Fig. 6. As can be seen, in this set of composite films in the studied range of concentration x of metallic phase $Co_{41}Fe_{49}Zr_{10}$ the $Z'(f)$ dependences have a sigmoidal shape that is characteristic for some of metal-dielectric nanocomposites with hopping mechanism of carrier transport in accordance with the model [24]. At the same time, we should mention negative sign of the phase shift angle θ in Fig. 6b, which indicates the predominance of the capacitive contribution to the reactive part of the admittance in the films deposited in an atmosphere of pure argon (probably due to relatively small amount of semiconducting iron oxides FeO and Fe_3O_4 [23,25] mentioned above).

The results of $Z'(f)$ and θ(f) measurements at the temperature 300 K for the films deposited in a gas mixture of argon and oxygen are presented in Fig. 7. As follows from Fig. 7a, in the studied x values, the sigmoid-like dependences of $Z'(f)$ begin to manifest itself only for composite films with $x > 70$ at.% and only at frequencies higher than 100 kHz. At the same time, in Fig. 7b for the samples with $x < 70$ at.% we observe the transition of θ(f) from negative to positive values when frequency increasing. The latter means the delay of the current with respect to the applied AC voltage, i.e. the effect of "negative capacity" occurs (prevailing inductive-like contribution over capacitive-like in imaginary part of admittance).

Describing the behavior of $Z'(f)$ and θ(f) dependences in the studied nanocomposites $(Co_{41}Fe_{49}Zr_{10})_x(SiO_2)_{100-x}$ of Set 1, when conducting nanoparticles have "core-shell" structure, from the point of view of the chemical composition, phase state and admittance, we also should note that the films obtained by deposition in pure argon atmosphere, can be divided into 3 areas: (i) the region below the "touching threshold" x_t = 47–48 at.% is related to the dielectric part of the insulator–metal transition, in which the metallic nanoparticles are separated by high-resistive interlayers of silicon oxide SiO_x; (ii) the region with $x > 67$–68 at.%, related to the metallic part of the insulator–metal transition, in which a highly conductive network of unoxidized "cores" of metal nanoparticles is formed; (iii) a region between the concentration x_t = 47–48 at.% and x_C = 67–68 at.%, in which a direct contact is formed between the oxide "shells" of the oxidized nanoparticles. Addition of oxygen to the deposition atmosphere in the vacuum chamber (the films of Set 2) shifts both percolation (x_C) and touching (x_t) thresholds to significantly higher concentrations x (approximately on 10 at.% every) than was observed in the films of Set 1, as well as in similar composite films $(FeCoZr)_x(Al_2O_3)_{100-x}$ and $(FeCoZr)_x(CaF_2)_{100-x}$ which used another matrixes [8–14,24,26–29].

Both observed features of $Z'(f)$ and θ(f) dependences indicate that the films deposited in the mixture of Ar and O_2 are oxidized more intensively than the films deposited in pure Ar gas. Moreover, as follows from Mossbauer, magnetization and XPS measurements [8–14,24,26–29], appearance of the "negative capacitance" at x less than touching threshold can be due to semiconducting character of prevailing iron oxide (FeO) as compared with insulating oxides (CoO, Co_3O_4, Fe_2O_3) around metallic "cores" $Co_{41}Fe_{49}Zr_{10}$ in nanoparticles with "core-shell" structure. As was shown in [24], the "core- shell" structure of CoFeZr nanoparticles in dielectric matrixes leads to realization of electron hopping between semiconducting parts of "shells" in nanoparticles and the formation of dipoles due to charge exchange. Just this leads to an increase in the effect of "negative capacitance" in such metal-dielectric composites.

4. Resume

Based on the complex analysis of chemical and phase composition, local ordering, magnetization, and admittance experiments, it was shown that $Co_{41}Fe_{49}Zr_{10}$ nanoparticles embedded into SiO_2 matrix, when depositing both in pure argon (Set 1) and in argon-oxygen gas mixture (Set 2), possess the "core-shell" structure, where "shell"

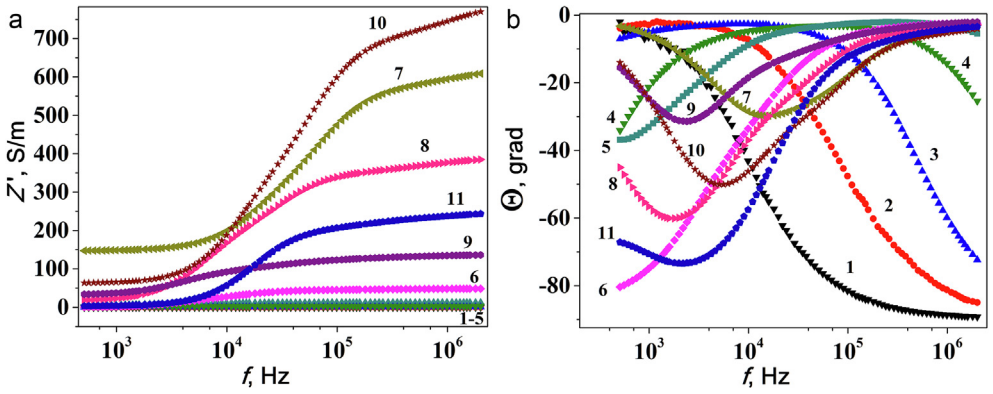

Fig. 6. Dependences of the active part of the admittance σ (a) and phase shift angle θ (b) on frequency f, measured at 300 K, for nanocomposite films $(Co_{41}Fe_{49}Zr_{10})_x(SiO_2)_{100-x}$ deposited in the atmosphere of pure argon: 38.1 (1); 42.0 at.% (2); 47.7 at.% (3); 53.4 at.% (4); 58.6 at.% (5); 62.8 at.% (6); 66.2 at.% (7); 68.5 at.% (8); 70.5 at.% (9) 73.4 at.% (10); 74.2 at.% (11).

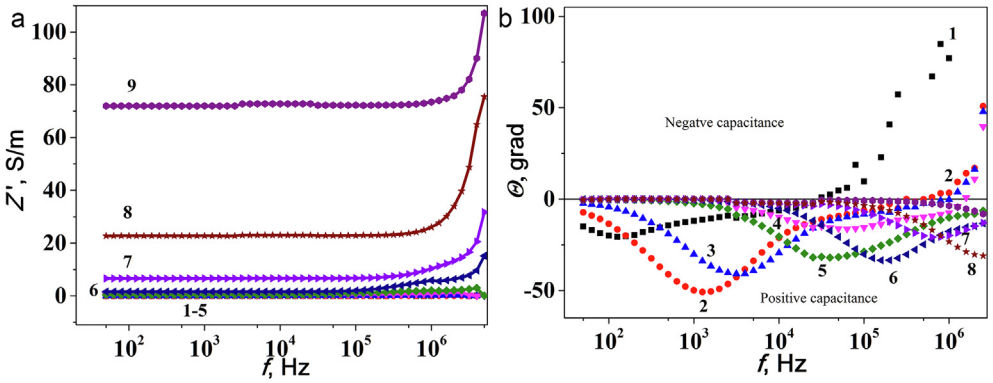

Fig. 7. Dependences of the active part of the admittance σ (a) and phase shift angle θ (b) on frequency *f*, measured at 300 K, for nanocomposite films $(Co_{41}Fe_{49}Zr_{10})_x(SiO_2)_{100-x}$ deposited in the mixture of argon and oxygen: 51.8 at.% (1); 58.2 at.% (2); 60.1 at.% (3); 67.0 at.% (4); 68.5 at.% (5); 74.0 at.% (6); 76.3 at.% (7); 79.7 at.% (8); 82.8 at.% (9).

consists of native iron and cobalt oxides. In the films $(Co_{41}Fe_{49}Zr_{10})_x(SiO_2)_{100-x}$ of Set 1, deposited in pure argon gas, in the reactive part of admittance at all frequencies the capacitive component at 300 K prevails. Deposition of the films $(Co_{41}Fe_{49}Zr_{10})_x(SiO_2)_{100-x}$ in argon-oxygen gas mixture (Set 2) causes additional oxidation of FeCoZr nanoparticles, resulting in prevailing of the inductive-like contribution over capacitive in the reactive part of admittance at 300 K and at frequencies above 10 kHz. The appearance of the "negative capacitance" effect indicates the prevailing of amount of semiconducting iron oxides (FeO) over the insulating oxides of iron and cobalt (CoO, Co_3O_4, Fe_2O_3) in "shells" around metallic "cores" $Co_{41}Fe_{49}Zr_{10}$ in nanoparticles with "core-shell" structure.

CRediT authorship contribution statement

J.A. Fedotova: Conceptualization. **A.V. Pashkevich:** Investigation. **Ali Arash Ronassi:** Methodology. **T.N. Kołtunowicz:** Conceptualization, Funding acquisition. **A.K. Fedotov:** Software. **P. Zukowski:** Writing - review & editing, Funding acquisition. **A.S. Fedotov:** Writing - review & editing. **J.V. Kasiuk:** Investigation. **Yu.E. Kalinin:** Writing - original draft. **A.V. Sitnikov:** Resources. **V.V. Fedotova:** Data curation. **A. Evtuh:** Validation.

Declaration of Competing Interest

The authors declare that they have no known competing financial interests or personal relationships that could have appeared to influence the work reported in this paper.

Acknowledgments

This research was partially funded from the Polish Ministry of Science and Higher Education from science fund of the Lublin University of Technology, at the Faculty of Electrical Engineering and Computer Science FN-28/E/EE/2019, entitled "*Researches of electrical, magnetic, thermal and mechanical properties of modern electrotechnical and electronic materials, including nanomaterials and diagnostic of electrical devices and their components*"

This research was also funded by the State program of scientific research "*Physical Materials Science, New Materials and Technologies*" (Belarus) under grant number 1.15.1. and by the Ministry of Education and Science of Ukraine, Ukraine in the framework of the program of bilateral cooperation between the Republic of Belarus and Ukraine in the field of science and technology (Grant No. M/21).

Appendix A. Supplementary data

Supplementary data to this article can be found online at https://doi.org/10.1016/j.jmmm.2020.166963.

References

[1] J. Fedotova, FeCoZr-Al2O3 granular nanocomposite films with tailored structural, electric, magnetotransport and magnetic properties, ed. B. Aktas, F. Mikailov, Springer Proceedings in Physics: Advances in nanoscale magnetism, Berlin, 122 (2008) 231–267.

[2] N.A. Poklonski, S.V. Shpakovski, N.I. Gorbachuk, S.B. Lastovskii, Negative capacitance (impedance of the inductive type) of silicon p^+-n junctions irradiated with fast electrons, Semiconductors 40 (2006) 803–807.

[3] M.B. Partenskii, P.C. Jordan, Negative capacitance and instability at electrified interfaces, Condens. Matter Phys. 8 (2) (2005) 397–412.

[4] G.B. Parravicini, A. Stella, M.C. Ungureanu, R. Kofman, Low-frequency negative capacitance effect in systems of metallic nanoparticles embedded in dielectric matrix, Appl. Phys. Lett. 85 (2004) 302–309.

[5] A.M. Saad, A.V. Mazanik, Yu.E. Kalinin, J.A. Fedotova, A.K. Fedotov, S. Wrotek, A.V. Sitnikov, I.A. Svito, Structure and electrical properties of CoFeZr-aluminium oxide nanocomposite films, Rev. Adv. Mater. Sci. 8 (2004) 34–40.

[6] A.M. Saad, B. Andrievsky, A. Fedotov, J. Fedotova, T. Figielski, Yu. Kalinin, V. Malyutina-Bronskaya, A Mazanik, A. Patryn, A. Sitnikov, I.A. Svito, AC and DC carrier transport in (FeCoZr)x(Al2O3)1 − x nanocomposite films for spintronic applications, Proceedings of SEMINANO 2005 (Budapest, Hungary, September 10-12, 2005) 321–324.

[7] M. Ershov, H.C. Liu, L. Li, M. Buchanan, Z. Wasilewski, A. Jonscher, IEEE Transact. on Electr. Dev. 45 (10) (1998) 2196–2206.

[8] A.M. Saad, A.K. Fedotov, I.A. Svito, J.A. Fedotova, V. Andrievsky, Yu.E. Kalinin, V.V. Fedotova, V. Malyutina-Bronskaya, A.A. Patryn, A.V. Mazanik, Impedance and magnetization of CoFeZr nanoclusters embedded into alumina matrix, J. Alloys Compds. 423 (2006) 186–1180.

[9] J. Fedotova, A. Saad, V. Fedotova, Yu. Ilyashuk, A. Fedotov, A. Larkin, Yu. Kalinin, A. Sitnikov, Influence of oxygen and nitrogen on impedance and magnetoimpedance of soft magnetic CoFeZr nanoparticles embedded in alumina matrix, Proceedings of 9th IEEE Conference on Nanotechnology, IEEE-NANO Genoa, July 26-30, 2009, 651–654.

[10] P. Zhukowski, T. Koltunowicz, J. Partyka, J.A. Fedotova, A.V. Larkin, Electrical properties of nanostructures $(CoFeZr)_x + (Al_2O_3)_{1-x}$ with use of alternating current, Vacuum 83 (2009) S275–S279.

[11] P. Zhukowski, T. Koltunowicz, J. Partyka, J.A. Fedotova, A.V. Larkin, Hopping conductivity of metal-dielectric nanocomposites produced by means of magnetron sputtering with the application of oxygen and argon ions, Vacuum 83 (2009) S280–S283.

[12] T.N. Koltunowicz, P. Zhukowski, J.A. Fedotova, A.V. Larkin, Inductive-type properties of (Co45Fe45Zr10)x(Al2O3)100 − x nanocomposites produced by the ion-beam sputtering in the argon and oxygen ambient, J. Nano Electron. Phys. 4 (1), (2012), P.01002-1–01002.

[13] A.V. Larkin, A.K. Fedotov, J.A. Fedotova, T.N. Koltunowicz, P. Zhukowski, Temperature and frequency dependencies of real part of impedance in the FeCoZr-doped PZT nanogranular composites, Mater. Sci.-Poland 30 (2) (2012) 75–81.

[14] Yu.E. Kalinin, A.V. Sitnikov, O.V. Stognei, I.V. Zolotukhin, P.V. Neretin, Electrical properties and giant magnetoresistance of CoFeB-SiO_2 amorphous granular composites, Mat. Sci. Eng. A304–306 (2001) 941–945.

[15] S. Sankar, A.E. Berkowitz, D.J. Smith, Spin-dependent transport of Co-SiO_2 granular films approaching percolation, Phys. Rev. B. 62 (21) (2000) 14273–14278.

[16] S. Mitani, H. Fujimori, S. Ohnuma, Spin-dependent tunneling phenomena in insulating granular systems, J. Magn. Magn. Mater. 165 (1–3) (1997) 141–148.

[17] B. Abeles, P. Sheng, M.D. Coutts, Y. Arie, Structural and electrical properties of granular metal films, Adv. Phys. 24 (1975) 407–461.

[18] M. Ohnuma, K. Hono, H. Onodera, J.S. Pedersen, S. Mitani, H. Fujimori, Distribution of Co Particles in Co-Al-O Granular Thin Films, J. Metastable Nanocryst. Mater. 1 (1999) 171–176.

[19] A. Williame, W.L. Johnson, The structure of some refractory transition metal-metalloid glasses, J. Non-Cryst. Solids 34 (1979) 121–126.

[20] K. Yakushiji, S. Mitani, K. Takanashi, J.-G. Ha, H. Fujimori, Composition dependence of particle size distribution and giant magnetoresistance in Co-Al-O granular films, J. Magn. Magn. Mater. 212 (2000) 75–81.

[21] G. Wastlbauer, J.A.C. Bland, Structural and magnetic properties of ultrathin

epitaxial Fe films on GaAs(001) and related semiconductor substrates, Adv. Phys. 54 (2) (2005) 137–219.
[22] Z.H. Wang, C.J. Choi, J.C. Kim, B.K. Kim, Z.D. Zhang, Characterization of Fe-Co alloyed nanoparticles synthesized by chemical vapor condensation, Mater. Lett. 57 (2003) 3560–3564.
[23] J. Chen, X. Wu, A. Selloni, Electronic structure and bonding properties of cobalt oxide in the spinel structure, Phys. Rev. B 83 (2011) 245204.
[24] P. Zukowski, T.N. Koltunowicz, O. Boiko, V. Bondariev, K. Czarnacka, J.A. Fedotova, A.K. Fedotov, I.A. Svito, Impedance model of metal-dielectric nanocomposites produced by ion-beam sputtering in vacuum conditions and its experimental verification for thin films of $(FeCoZr)_x(PZT)_{(100-x)}$, Vacuum 120 (2015) 37–43.
[25] R.M. Cornell, U. Schwertmann, The iron oxides: Sructure, Properties, Reactions, Occurrence and Uses, 2nd, Completely Revised and Extended Edition, WILEY-VCH GmbH & Co, KGaA, 2006.
[26] J. Kasiuk, J. Fedotova, J. Przewoznik, M. Sikora, Cz. Kapusta, J. Żukrowski, A. Grce, M. Milosavljević, Oxidation controlled phase composition of FeCo(Zr) nanoparticles in CaF_2 matrix, Mater. Charact. 113 (2016) 71–81.
[27] I.A. Svito, A.K. Fedotov, A. Saad, M. Milosavljevic, J.A. Fedotova, T.N. Koltunowicz, P. Zhukowski, Low-Temperature DC Carrier Transport in $(Fe_{0.45}Co_{0.45}Zr_{0.10})_x(Al_2O_3)_{1-x}$ Nanocomposites Manufactured by Sputtering in Pure Ar Gas Atmosphere, Adv. Condens. Matter Phys. 2015 (2015) 320187.
[28] T.N. Koltunowicz, P. Zhukowski, A.K. Fedotov, A.V. Larkin, A. Patryn, B. Andriyevskyy, A. Saad, J.A. Fedotova, V.V. Fedotova, Influence of matrix type on negative capacitance effect in nanogranular composite films FeCoZr-Insulator, Elektronika ir Elektrotechnika 19 (2013) 37–40.
[29] I.A. Svito, A.K. Fedotov, A. Saad, T.N. Koltunowicz, P. Zhukowski, Low-temperature DC carrier transport in $(Co_{0.45}Fe_{0.45}Zr_{0.10})_x(Al_2O_3)_{1-x}$ nanocomposites sputtered in mixed argon-oxygen atmosphere, Acta Phys. Pol. A 125 (2014) 1351–1354.